Fuel 332 (2023) 126337

Contents lists available at ScienceDirect

Fuel

journal homepage: www.elsevier.com/locate/fuel

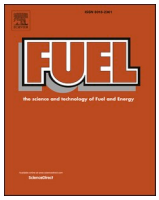

Full Length Article

Optical in-situ measurements and modeling of post-flame sulfation of NaOH (g) and NaCl(g)

Daniel Schmid [a,*], Wubin Weng [b], Shen Li [b], Oskar Karlström [a,c], Mikko Hupa [a], Zhongshan Li [b], Peter Glarborg [d], Paul Marshall [e], Marcus Aldén [b]

[a] Group of Inorganic Chemistry, Johan Gadolin Process Chemistry Centre, Åbo Akademi University, Henrikinkatu 2, 20500 Turku, Finland
[b] Division of Combustion Physics, Lund University, P.O. BOX 118, SE-221 00 Lund, Sweden
[c] Industrial Engineering and Management, Department of Mechanical and Materials Engineering, University of Turku, Finland
[d] Department of Chemical Engineering, Technical University of Denmark, Kgs. Lyngby DK-2800, Denmark
[e] Department of Chemistry and Center for Advanced Scientific Computing and Modeling, University of North Texas, Denton, TX 76203-5070, USA

ARTICLE INFO

Keywords:
Sodium sulfation
Alkali sulfation
UV absorption spectroscopy
Chemical kinetic modeling

ABSTRACT

Post-flame sulfation of gaseous sodium hydroxide (NaOH) and sodium chloride (NaCl) was investigated with optical in situ measurements at 850 to 1475 °C. A multi-jet burner was used to generate well-controlled combustion environments. The multi-jet burner also enabled the separate feeding of the sodium species and SO_2 to the combustion environment where the sulfation reactions occurred. Concentrations of NaOH(g) and NaCl(g) were measured in the product gas using broadband UV absorption spectroscopy to follow the degree of sulfation. At 1475 and 1275 °C almost no sulfation occurred with an initial NaOH(g) concentration of 20 ppm and SO_2 concentrations between 0 and 150 ppm. At 985 °C, the NaOH(g) concentration decreased to less than 5 ppm with SO_2 concentrations above 50 ppm and at 850 °C almost all NaOH(g) was sulfated under these conditions. The experimental results for the gas-phase sulfation of NaOH were compared to previous results for the sulfation of KOH under the same conditions and the results were shown to be similar for NaOH and KOH under these conditions. Sulfation of NaOH(g) generally occurred to a more significant extent than the sulfation of NaCl(g). At 1115 to 1475 °C, no sulfation of NaCl(g) was observed. At the lowest investigated temperature, 850 °C, the NaCl (g) concentration decreased from 20 ppm to 12 ppm after the addition of 150 ppm SO_2. Chemical equilibrium calculations and kinetic modeling using an updated kinetic model for the detailed Na-Cl-S chemistry were compared to the experimental results. Above 1100 °C, the system can be described by chemical equilibrium, implying that equilibrium is reached in less than 100 ms. At temperatures below 1100 °C, the measured concentration indicated kinetic control. Under these conditions, the kinetic model was in good agreement with the experimental results for NaOH(g) but over-predicted the sulfation of NaCl(g). The combined experimental data, chemical equilibrium calculations and kinetic modeling of the present study support that sulfation of alkali species can occur in the gas phase through homogeneous reactions.

1. Introduction

High-temperature chemistry of alkali species is of interest due to its importance in aerosol formation, deposition, and corrosion in combustion and gasification of challenging fuels such as solid biomass, a range of various waste side streams and black liquor [1–4]. This range of fuels often contain high amounts of alkali, sulfur and chlorine, which can be released as alkali chloride, alkali hydroxides, hydrogen chloride (HCl) and sulfur dioxide (SO_2) [5–8]. Alkali compounds, such as alkali chlorides, contribute to slagging, fouling and corrosion [9,10,11]. Both sodium chloride (NaCl) and potassium chloride (KCl) are highly corrosive towards conventional heat exchanger materials [12]. Corrosion on metal surfaces can be minimized and even eliminated when the alkali compounds are converted to alkali sulfates due to their higher melting points. The sulfation reactions can occur with SO_2 released from the fuel. If the sulfur content in the fuel is low, however, additional sulfur-containing compounds can be added to increase the degree of sulfation. One possibility is the addition of elemental sulfur, which is then

* Corresponding author.
E-mail address: dschmid@abo.fi (D. Schmid).

https://doi.org/10.1016/j.fuel.2022.126337
Received 10 July 2022; Received in revised form 19 September 2022; Accepted 10 October 2022
Available online 13 October 2022

oxidized to SO_2 in thermal conversion [13], or the co-combustion with sulfur-rich fuels like peat [14]. Another possibility is the introduction of sulfates, e.g. ammonium or ferric sulfate, which will decompose to SO_3, which has been shown to be more efficient for sulfation reactions with alkali as compared to SO_2 [15–17].

The formation of alkali sulfates is believed to occur both in the gas phase and in the condensed phase, dependent on the temperature [18–20]. Sulfation in the gas phase may be expected to occur at faster rates than in the solid and liquid phases [18]. Glarborg and Marshall [21] proposed a detailed kinetic mechanism for the formation of gaseous alkali sulfates, including reactions between gaseous alkali chlorides and hydroxides with sulfur oxides. Predictions based on this mechanism for the sulfation of KCl were in good agreement with experimental results from an entrained flow reactor of Iisa et al. at 900–1100 °C [18]. Results of that study suggest that most of the potassium sulfation at temperatures above 900 °C occurs in the gas phase.

In the sulfation of KCl, SO_3 plays a key role [18]. Jiménez and Ballester emphasized that the kinetics of the oxidation of SO_2 to SO_3 has been the main obstacle for the complete description of sulfate formation [22]. SO_3 initiates sulfation of alkali species [21]:

$$NaCl + SO_3 (+M) \rightleftharpoons NaSO_3Cl (+M) \quad (R1)$$

$$NaOH + SO_3 (+M) \rightleftharpoons NaHSO_4 (+M) \quad (R2)$$

$$NaSO_3Cl + H_2O \rightleftharpoons NaHSO_4 + HCl \quad (R3)$$

$$NaHSO_4 + NaCl \rightleftharpoons Na_2SO_4 + HCl \quad (R4)$$

$$NaHSO_4 + NaOH \rightleftharpoons Na_2SO_4 + H_2O \quad (R5)$$

Hindiyarti et al. [1] suggested that the rate of SO_2 oxidation to SO_3 may be too slow at lower temperatures and presented alternative sulfation pathways. Accordingly, sulfation can be initiated by a direct reaction between NaOH and SO_2, forming a sulfite species (R6) which can then be oxidized to bisulfate (R7), with the oxidation of the sulfite as the rate-limiting step.

$$NaOH + SO_2(+M) \rightarrow NaHSO_3(M) \quad (R6)$$

$$NaHSO_3 + O_2 \rightarrow NaHSO_4 + O \quad (R7)$$

Various studies have investigated the details of the K-Cl-S chemistry, both with experimental work and modeling in laboratory and larger scale [23–25]. Weng et al. developed an experimental measurement system to study gas-phase sulfation and homogeneous nucleation of alkali compounds, based on a novel multi-jet burner being able to provide well-controlled conditions, using optical in situ measurements to quantify relevant species [26–28]. Sulfation experiments were performed feeding K_2CO_3 or KCl together with SO_2 to a hot and stable gas environment. Key species such as KOH, KCl and K atoms were quantified in the gas phase to determine their formation and consumption, and the sulfation was indirectly determined based on measured concentrations of KOH and KCl. The experimentally determined concentrations were compared to predictions by a detailed K-Cl-S mechanism based mostly on the work by Glarborg and Marshall [21]. The model predictions were in satisfactory agreement with the experimental results.

Previous work on gas-phase sulfation of alkali salts have largely focused on potassium, which is the dominating alkali element in most biomass fuels. Besides high potassium contents, many biomasses and wastes (and also some coals [29]) have high sodium contents, e.g. algae and black liquor (one of the most used biomass based fuels) have high sodium contents.

The objective of the present work is to clarify the homogeneous Na-Cl-S chemistry in the gas phase at high temperatures between 850 and 1475 °C. This temperature range is relevant for most combustion processes, ranging from grate fired combustion and fluidized bed combustion to pf combustion. The sulfation of NaOH and NaCl was investigated experimentally in a multi-jet burner, and the consumption of NaOH and NaCl in the gas phase by reaction with SO_2 was determined using UV absorption spectroscopy. The sulfation reactions of sodium species have not been investigated previously under such conditions. A new updated kinetic Na-S-Cl model is also tested under the investigated conditions. The model is based on the work of Glarborg and Marshall [21], but updated in the present work with novel thermodynamic data and added reaction pathways. In addition, chemical equilibrium calculations are performed to evaluate whether the set-up operates at non-equilibrium conditions.

2. Experimental

A multi-jet burner (see Fig. 1) was used to create well-controlled high temperature conditions for the sodium sulfation experiments. A more detailed description of the reactor setup can be found elsewhere [31]. The multi-jet burner consists of 181 jet tubes through which a gas mixture of methane, oxygen and air was fed. Above each jet, a laminar conical flame is formed. A co-flow is introduced through a perforated mask and several layers of glass beads with a diameter of 1 mm, which is evenly mixed with the hot gas products from the jet tubes, creating a fairly homogeneous hot flue gas environment above the burner outlet for a given temperature and oxygen concentration, depending on the composition of the used gas mixtures. The burner outlet is 29 mm above the front of the jet tubes. The burner walls are insulated to minimize heat loss.

Table 1 lists the compositions of the used gas mixtures and temperatures and concentrations in the zone above the burner where the optical measurements took place. The temperature was measured using two-line atomic fluorescence (TLAF) thermometry using indium atoms, with a reported accuracy of ~ 2.7 % [32]. Additional measurements were obtained with a B-type thermocouple (OMEGA) with a wire diameter of 0.25 mm [26], corrected for radiation loss based on a model reported by Weng et al. [31]. The emissivity of the thermocouple was adjusted so that the thermocouple gave the same temperature at 40 mm height as the temperature from the TLAF measurement. The temperature was measured in the hot flue gas without NaOH, NaCl or SO_2 seeding to avoid any particle deposition effect and to minimize catalytic effects of the thermocouple. The temperature profiles along the vertical axis and adiabatic flame temperatures can be found in the supplementary material.

For the experiments with NaCl and NaOH, respectively, 1.0 M NaCl or 0.5 M Na_2CO_3 solutions were fed to the jet chamber. The Na_2CO_3 was rapidly converted to NaOH by reaction with H_2O when the temperature increased. An ultrasonic fog generator was placed in the flask with the Na-containing solution, and the fog was then transported to the jet chamber via an air flow of 0.5 Nl/min. In the jet chamber, the Na-containing fog was mixed with the methane/air/oxygen mixture and fed to the jet outlet, where NaOH(g) or NaCl(g) was formed after passing the flame. To prevent SO_2 and sodium reacting already in the jet chamber, SO_2(g) was fed to the burner via the co-flow and the sulfation raction was limited by the mixing rate. For each experiment, the NaOH or NaCl concentration in the hot flue gas was measured by the below described UV absorption spectroscopy, before, while and after SO_2 has been added. This was to ensure that the volume fraction of NaOH or NaCl transported into the flame is the same as set. Since the seeding of SO_2 was conducted only for a short time period, the seeding fluctuation should be small when the NaOH or NaCl was the same for the measurement before and after the SO_2 addition.

NaOH(g) and NaCl(g) were quantified 5 mm above the burner outlet (about 4 cm downstream of the small jet flames) using broadband UV absorption spectroscopy (see Fig. 1c). At this stage the gases were fully mixed and the gaseous NaOH and NaCl were distributed evenly, hence it is reliable to use the line-of sight measurement for the quantification of NaOH and NaCl concentrations in the flame. The distribution has been investigated previously [33]. The UV beam had a diameter of 10 mm and was generated by a deuterium lamp (L1313, Hamamatsu). The beam

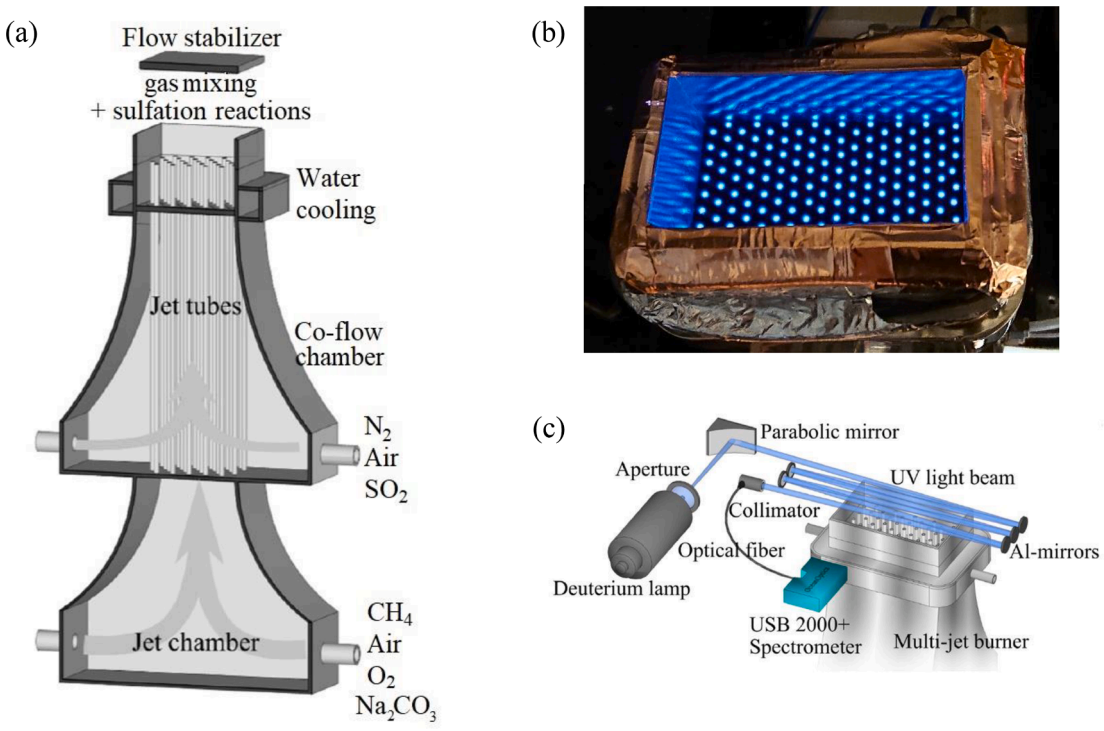

Fig. 1. Schematic picture of the Multi-Jet Burner at Lund University (a) (reproduction from [28]), top view on pre-mixed flames on the outlets of the jet tubes (b) and setup for broadband UV absorption spectroscopy system (c) (reproduction from [30]).

Table 1
Gas-flow composition and gas product temperature 5 mm above the burner outlet; temperature and gas concentration refer to the zone where the sulfation experiments take place.

Temp. [°C]	Fuel-oxygen ratio φ	Gas flow rate [Nl/min]					Gas conc. [%]			
		Jet-flow				Co-flow				
		CH_4	Air	O_2	N_2	Air	O_2	CO_2	H_2O	N_2
1475	0.74	2.66	17.34	1.89	10.83	7.74	4.5	6.5	13.2	75
1275	0.70	2.47	12.23	2.58	18.97	8.90	4.6	5.4	11.0	79
1115	0.67	2.38	11.89	2.26	22.69	9.83	4.6	4.6	9.4	81
985	0.63	2.09	10.90	2.07	26.50	10.66	5.2	3.9	7.9	83
850	0.60	1.71	8.91	1.69	26.92	10.25	4.6	3.4	6.9	85

was passed five times through the hot flue gas by five UV-enhanced aluminium mirrors to achieve a high sensitivity with a long optical path length. The light was then collected and anlyzed with a spectrometer (USB 2000+, Ocean Optics). 200 scans were performed for each experiment with an integration time of 2 ms and each experiment was repeated 20 times.

The concentrations of NaOH (g) and NaCl (g) were determined using the Beer-Lambert law.

$$Absorbance(\lambda) = N_A \sigma_A(\lambda) L = -\ln\left(\frac{I_s(\lambda)}{I_0(\lambda)}\right) \quad (1)$$

where λ is the wavelength; $I_s(\lambda)$ and $I_0(\lambda)$ are the intensities of the UV light after the hot flue gas and the UV light source, respectively, at a given wavelength; N_A is the number density of the gas species; $\sigma_A(\lambda)$ is the absorption cross section at a given wavelength and L is the optical path length.

The cross-section data used in the present study is based on previous work from Weng et al. [27,34] The absorption cross sections for NaOH and NaCl were determined between 1125 and 1575 °C [27]. The temperature dependence of the absorption cross section in this temperature range is weak and, thus, it is reasonable to also use the same absorption cross section for 850 and 985 °C. Almost the same concentrations for NaOH or NaCl were measured at different temperatures with the same feeding rate of alkali, which supports that the value for the absorption cross sections measured at 1125–1575 °C can be used for the investigated temperature range in the present study. For NaOH, the absorption peaks occur at 230 and 320 nm with $\sigma_{230} = 1.67{\cdot}10^{-17}$ cm^2/molecule and $\sigma_{320} = 1.29{\cdot}10^{-17}$ cm^2/molecule.

According to the Beer-Lambert law, the uncertainty of the measurement originated from the uncertainty of the cross section data, optical path length and the measurement of the absorbance. The uncertainty of the cross-section data is about ± 5 % [34]. The optical path length was estimated based on previous visualization of KOH distribution [33], adding an additional uncertainty of ± 10 % due to uneven distribution at the edge of the flue gas. The uncertainty from the absorbance measurement is small compared to the uncertainties for the cross section and optical path length and is hence neglected for the overall uncertainty. The reaction influence by the UV radiation is negligible as well. Since the UV light beam had a diameter of about 10 mm and the hot flue gas was flowing at a speed of around 1 m/s, the molecules and radicals only experiences 10 ms radiation from the UV light, and the UV light only had an irradiance below 0.1 $\mu W{\bullet}cm^{-2}{\bullet}nm^{-1}$. It was estimated that only about 0.001 % of the NaOH molecules were excited by the UV light in the experiment. Summing up,

the uncertainty of the measurement was estimated to be ± 15 %.

Fig. 2a shows the absorption spectrum of NaOH and Fig. 2b shows the overlapping absorption spectrum of NaCl and NaOH present in the NaCl seeded flame at 1275 °C with the addition of 20 ppm SO_2. Corresponding figures at same conditions without addition of SO_2 are shown in Fig. 2 and Fig. 3 of the supplementary material to illustrate that SO_2 does not interfere with the measurement as it is subtracted from the spectrum via background measurements. To quantify NaCl and NaOH simultaneously, in a first step the NaOH concentration was determined from the peak at 320 nm of the 'raw data (NaOH + NaCl spectrum)', as this peak is not overlapping with the spectrum of NaCl. Based on this NaOH concentration, the entire spectrum for NaOH ('NaOH (fitted based on absorption at 320 nm)' in Fig. 2b) was fitted using the cross section at different wavelengths obtained from [27]. In a second step, the NaOH absorbance was then subtracted from the combined spectrum ('raw data (NaOH + NaCl spectrum)' in Fig. 2b) to obtain the absorbance for NaCl ('NaCl (difference between raw data and NaOH fit)' in Fig. 2b). The NaCl concentration was then determined from the absorption peak at 238 nm with the absorption cross section $\sigma_{238} = 2.5{\cdot}10^{-17}$ cm^2/molecule.

3. Model

The thermodynamic data and reaction mechanism for sulfation of NaCl and NaOH were based on the work by Glarborg and Marshall [21], but updated as part of the present work. Glarborg et al. emphasized the importance of alkali hydrogen sulfates as gas-phase precursors of A_2SO_4, and estimated the thermodynamic properties of $KHSO_4$ and $NaHSO_4$, as well as chlorinated intermediates, from ab initio computations. In a later work, Hindiyarti et al. [1] proposed a number of additional pathways to sulfation of KCl and KOH, involving $KHSO_3$ and $KOSO_3$, and more recently, additional modifications were made to the potassium subset [25,26,28]. In the present work, these modifications have been applied also to the sodium subset. Using the methods described in ref. [21], with G3 theory replaced by G4 [35], properties for species added to the mechanism, i.e., $NaHSO_3$ and $NaOSO_3$ were calculated in the present work, and data for $NaSO_3Cl$ were updated. For the added reactions, rate constants were assumed to be similar for corresponding sodium and potassium reactions in the exothermic direction. Compared to the model of Glarborg and Marshall [21], the thermodynamic data for NaOH was replaced with data from the reference [36]. The novel calculated thermodynamic properties are listed in Table 2. In the Na-mechanism, a check was made to ensure that rate constants in both the forward and reverse direction were below the collision frequency.

The kinetic modeling was done with Chemkin-Pro. In a first step, a one-dimensional free propagation model was used to determine the composition of the post-flame gases. The mixture of these post-flame gases and the co-flow was used as the inlet gases for the plug flow reactor model that was used to model the sulfation reactions. In this step, 20 ppm NaOH or NaCl was added together with 0–150 ppm SO_2 to the hot gas products. For the plug flow model it was assumed that the post-flame gases and co-flow gases are mixed rapidly. The temperature profile in the model was adopted from the measured values.

FACTSAGE 7.3 was used for the equilibrium calculations. The "Equilib" module within the FACTSAGE software calculated the equilibrium concentrations by minimizing the Gibbs energy. All species that were considered for the kinetic model were also considered in the equilibrium calculations. The thermodynamic data was taken from the FACTSAGE database and extended with thermodynamic data for the following sodium species from reference [21] and from the present work: $NaSO_2$, $NaSO_3$, $NaSO_4$, $NaHSO_3$, $NaHSO_4$ and $NaSO_3Cl$.

4. Experimental results

It is a limitation in the present reactor setup, from a kinetic point of view, that the species could only be quantified 5 mm above the burner outlet and not close to the jet tubes due to the walls of the burner that are needed to stabilize the flames. Nevertheless, the measurements provide the first direct characterization of sulfation of sodium salts, and allow for an assessment of the relative importance of kinetic and equilibrium constraints.

Fig. 3a presents the measured NaOH(g) concentrations above the burner outlet during the sulfation experiments at 850 to 1475 °C and for SO_2 concentrations between 0 and 150 ppm. The NaOH(g) concentration, without SO_2, is 20 ppm. The error bars in Fig. 3 are derived from the deviation of repeated experiments and from the uncertainty of the measurement method. At the highest investigated temperature, 1475 °C, the NaOH(g) concentration remains constant at 20 ppm, indicating that no sulfation reactions take place under these conditions. When the temperature is reduced to 1275 °C, the NaOH(g) concentration decreases slightly with the addition of > 50 ppm SO_2. At 1115 °C, only little NaOH(g) was consumed with 20 ppm SO_2, but up to 40 % of the NaOH(g) was consumed with 100 or 150 ppm SO_2. Also at the lowest temperatures, 985 and 850 °C an increased NaOH(g) consumption with increased SO_2 concentration can be observed. At 850 °C, almost all NaOH(g) is consumed at SO_2 concentrations > 50 ppm. For comparison, experimental results from KOH sulfation under the same conditions, published by Weng et al [28], are shown in Fig. 3b. It can be seen that the consumption of the two alkali hydroxides is almost identical under same conditions. The consumption of NaOH(g), similar to KOH(g), can be explained by the sulfation of the NaOH(g) into gaseous Na_2SO_4 and

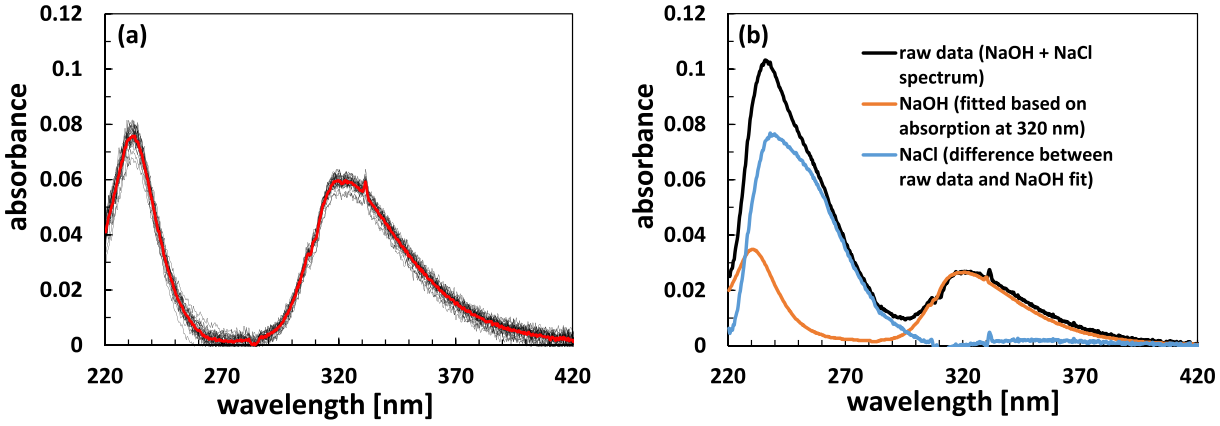

Fig. 2. (a) Measured absorbance of NaOH at 1275 °C adding 20 ppm NaOH and 20 ppm SO_2 to the flame (20 repetitions, red line showing the average absorbance) and (b) measured absorbance of combined NaOH and NaCl and calculated absorbance for NaOH and NaCl determined from the combined spectrum at 1275 °C adding 20 ppm NaCl and 20 ppm SO_2 to the flame. (For interpretation of the references to colour in this figure legend, the reader is referred to the web version of this article.)

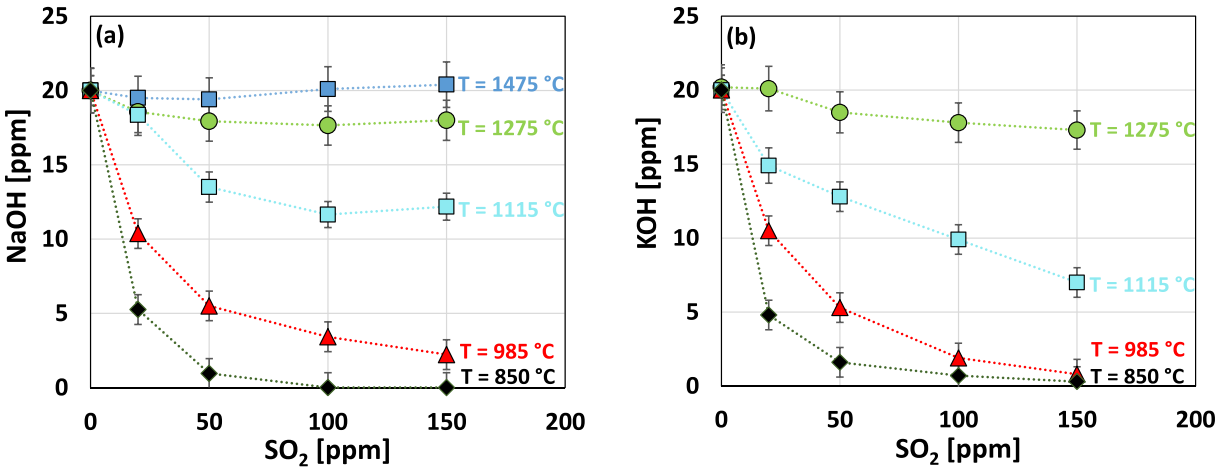

Fig. 3. (a) NaOH concentrations from sulfation experiments at various temperatures with 20 ppm NaOH inlet concentration and SO_2 concentrations between 0 and 150 ppm and (b) KOH concentrations from previous sulfation experiments under same conditions for comparison (KOH results reproduced from [28], dotted lines for clarity only).

Table 2
Thermodynamic properties calculated in the present work for selected alkali species. Units are cal, mol, K.

Species	$H_{f,298}$	S_{298}	$C_{p,300}$	$C_{p,400}$	$C_{p,500}$	$C_{p,600}$	$C_{p,800}$	$C_{p,1000}$	$C_{p,1500}$
$NaHSO_3$	−159.84	78.54	21.25	23.66	25.32	26.46	27.82	28.66	29.92
$NaOSO_3$	−159.88	79.27	22.07	24.80	26.69	27.97	29.42	30.19	31.08
$NaSO_3Cl$	−178.68	82.80	22.74	25.04	26.74	27.98	29.45	30.15	31.00

Na_2SO_4 aerosols, as proposed by Glarborg and Marshall [21].

The formation of sulfate aerosols from the sulfation of KOH(g) was detected previously at 985 and 850 °C by elastic scattering measurements [28]. Due to the similar experimental results for NaOH(g) and KOH(g), it is assumed that aerosol formation also takes place at these temperatures in the sulfation of NaOH(g). These results are also in agreement to results by Jiménez and Ballester [37]. In their study on pulverized olive residue combustion, it was observed that KOH was consumed in the presence of SO_2, and the nucleation of the formed K_2SO_4 started when temperatures decreased below 1000 °C.

Fig. 4 shows the concentrations of NaCl(g) and NaOH(g) above the burner outlet from the experiments with NaCl-seeding without SO_2. At low temperatures, all sodium in the gas-phase is present as NaCl(g). At increasing temperatures however, NaCl was partly converted to NaOH (g). At 1475 °C, around 50 % of the NaCl reacted to NaOH(g).

The NaCl(g) concentration for the sulfation experiments with NaCl-feeding are presented in Fig. 5. For the temperatures between 1115 and 1475 °C, it can be seen that the NaCl(g) concentration is not influenced by SO_2, hence no sulfation of NaCl(g) occurred under these conditions. At 985 °C, the NaCl(g) concentration decreased from roughly 17 ppm without SO_2 to roughly 12 ppm with 150 ppm SO_2. At lower SO_2 concentrations, the concentration remained at around 17 ppm. Only at the lowest temperature, i.e. at 850 °C, a continuous decrease in the NaCl(g) concentration with increasing SO_2

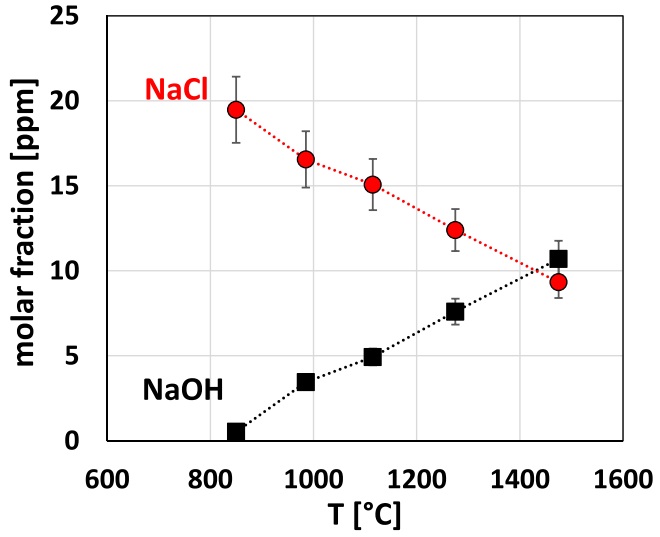

Fig. 4. Concentrations of NaCl and NaOH at 850–1475 °C measured in tests without SO_2 inlet concentration in all cases 20 ppm NaCl (dotted lines for clarity only).

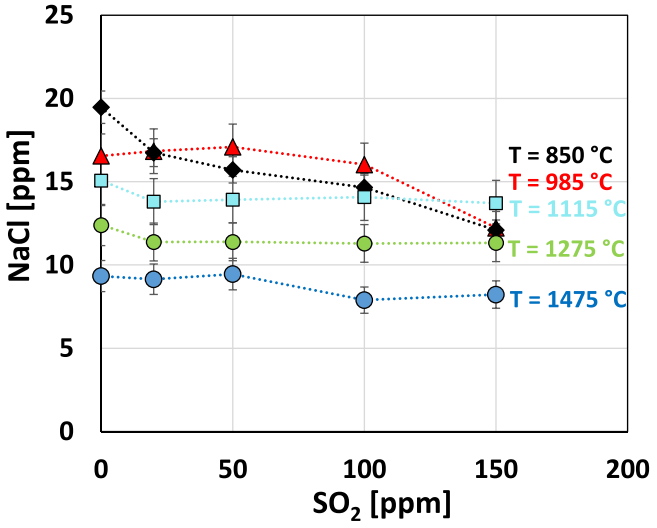

Fig. 5. NaCl concentrations from sulfation experiments at various temperatures with 20 ppm NaCl inlet concentration and SO_2 concentrations between 0 and 150 ppm (dotted lines for clarity only).

concentrations can be observed. The concentration decreases continuously from 20 ppm without SO_2 addition to roughly 12 ppm with 150 ppm SO_2, which corresponds to a reduction of around 40 %. It can be concluded that the sulfation of NaCl(g) occurs to a much lower extent as compared to the sulfation of NaOH(g) under the investigated conditions.

5. Modeling

Kinetic modeling and equilibrium calculations were made to further interpret the reactions occurring during the gas phase sulfation of NaOH and NaCl. Fig. 6 compares NaOH concentrations (a) and NaCl concentrations (b) from chosen experiments with predictions from the kinetic model and the thermodynamic model. In these sulfation tests, it can be seen that predictions from the kinetic model and the equilibrium calculations are almost identical at 1275 and 1475 °C, indicating that the system is already at equilibrium under the used conditions. For the cases at 1115 °C and below, the system seems not to be at equilibrium under the present conditions. At these temperatures, NaOH(g) are close to the values obtained from the kinetic model as compared to the equilibrium calculations. NaCl(g) concentrations in Fig. 6b are given for the cases at 985 and 850 °C, which are the only temperatures at which NaCl(g) sulfation was observed in the experiment. According to the modeling, the system is almost at equilibrium at 985 °C, but far from equilibrium at 850 °C. This is in agreement with previous findings for the sulfation of alkali chlorides, e.g. in the field study by Christensen and Livbjerg focusing on the sulfation of KCl, which also was far from equilibrium according to their model [38]. At 850 °C, where reactions seem to be limited by kinetics, the kinetic model does not give a good prediction and deviates significantly from the observations in the experiment.

A sensitivity analysis has been performed to illustrate the effects of uncertainties in the experimental setup and their effect on the modeling results. The results are shown in Fig. 4 of the supplementary material. In addition to the SO_2 inlet level, the flame temperature was found to be the most sensitive input parameter with a change of 40 °C sufficient to significantly alter the predicted NaOH concentration.

Generally, the model gives a good description of the observed sodium sulfation reaction. However, due to the fact that reactions occur rapidly, the current set-up cannot be used to fully validate the kinetic model. Nevertheless, the model gives a good kinetic description for most of the cases.

Fig. 7 shows concentrations of relevant species during NaOH(g) sulfation at 1115 °C with 50 ppm SO_2 as a function of time (logarithmic plot) and as a function of the distance from the jet-tubes (linear plot). It can be seen some reactions occur rapidly within the first 1 ms/ few millimeters above the burner outlet. After the rapid reactions in the beginning, NaOH is slowly consumed, while the concentration of Na_2SO_4 is steadily increasing. The range in which the optical measurement takes place (after roughly 30 ms reaction time) is marked by the dotted lines. Even beyond that range sulfation reactions seem to continue, indicating that indeed kinetics is investigated under these conditions and equilibrium has not been reached.

To clarify whether sulfation reactions take place in the gas phase and if stable gaseous products can be formed under these conditions, equilibrium calculations have been made to determine the ratio between gaseous and condensed Na_2SO_4. Fig. 8 shows the ratio of Na_2SO_4 (g) and Na_2SO_4 (l) between 890 and 1130 °C. Above 1080 °C, only the gaseous product seems to be stable. At below 1000 °C, almost all Na_2SO_4 is expected to be in the condensed phase. This is in agreement with the observations made by Weng et al. [28], reporting aerosol formation in alkali sulfation experiments at similar temperatures. The combined experimental data, chemical equilibrium calculations and kinetic modeling of the present study support that sulfation of alkali species can occur in the gas phase through homogenous reactions, in contrast to earlier reports [39].

6. Conclusions

Post-flame sulfation of NaOH(g) and NaCl(g) was investigated with optical in-situ measurements under well-defined combustion environments. Experiments were performed under oxidizing conditions at 850 to 1475 °C with initial concentrations of 20 ppm for the Na-species and 0–150 ppm SO_2. The concentrations of NaOH(g) and NaCl(g) were quantified using UV absorption spectroscopy. Additionally, an updated model for the detailed Na-Cl-S chemistry was used to describe the sulfation reactions.

At the highest investigated temperatures 1475 and 1275 °C almost no sulfation of NaOH(g) was observed in the experiments while almost all NaOH(g) was consumed with 50 ppm SO_2. The experimental results for the sulfation of NaOH(g) were compared to previous results for the sulfation of KOH(g) under the same conditions. The results for NaOH(g) were shown to be similar to those of KOH(g), indicating that the kinetics and thermodynamics are similar for those species under the investigated conditions.

Sulfation of NaCl(g) occurred to a much lower extent under the investigated conditions as compared to sulfation of NaOH(g). Sulfation of NaCl(g) was observed at 985 and 850 °C. At 850 °C the NaCl(g) concentration decreased from 20 to 12 ppm after the addition of 150 ppm SO_2.

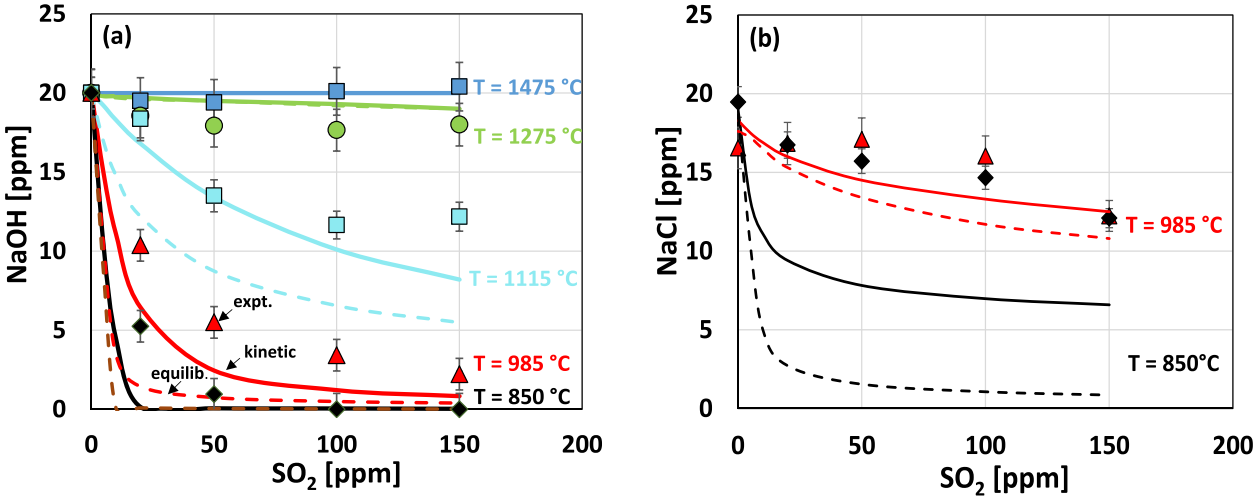

Fig. 6. (a) NaOH and (b) NaCl concentrations for sulfation experiments at 850 to 1475 °C and varying SO_2 concentrations; inlet concentration 20 ppm NaOH or 20 ppm NaCl respectively (dotted lines = equilibrium calculations, continuous lines = kinetic modeling and symbols = experimental results).

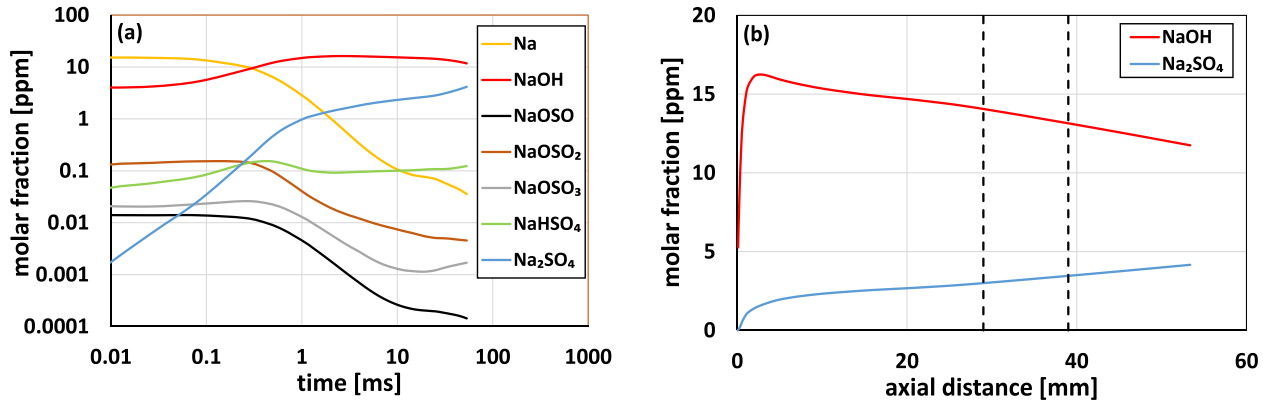

Fig. 7. (a) Molar fractions of relevant species as a function of time (logarithmic scale) and (b) molar fraction of NaOH and Na_2SO_4 (linear scale) from kinetic modeling of NaOH-sulfation experiments at 1115 °C as a function of the vertical distance from the jet-tubes (linear); inlet concentration 20 ppm NaOH and 50 ppm SO_2. The dotted lines indicate the area in which the optical measurement of NaOH was performed.

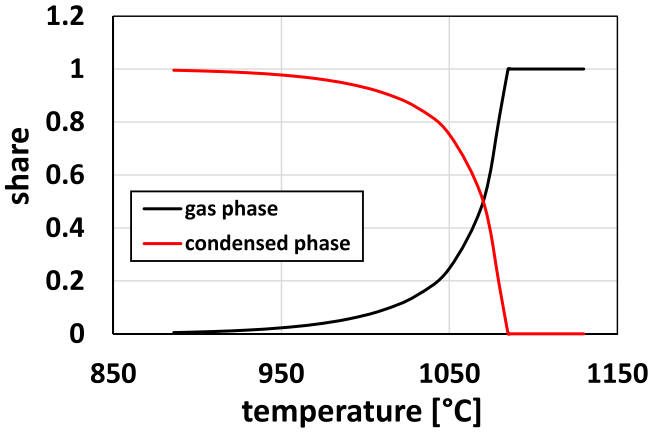

Fig. 8. Equilibrium ratio of Na_2SO_4(g) and Na_2SO_4 (l) for NaOH sulfation at 890 to 1130 °C; inlet concentration 20 ppm NaOH, 50 ppm SO_2, 4.7 % CH_4 and 13.9 % O_2 (N_2 as balance).

Chemical equilibrium calculations and kinetic modeling using an updated kinetic model for the detailed Na-Cl-S chemistry were compared to the experimental results. Above 1275 °C, the system can be described by chemical equilibrium, implying that equilibrium is reached in less than 50 ms. At 1115 °C and below, the measured concentrations were in good agreement to the updated chemical kinetic model. Under these conditions, the kinetic model was in good agreement with the experimental results for NaOH(g) but over-predicted the sulfation of NaCl(g). The combined experimental data, chemical equilibrium calculations and kinetic modeling support that sulfation of alkali species can occur in the gas phase through homogenous reactions.

CRediT authorship contribution statement

Daniel Schmid: Investigation, Writing – original draft. **Wubin Weng:** Methodology, Writing – review & editing. **Shen Li:** Investigation. **Oskar Karlström:** Writing – review & editing, Supervision, Project administration. **Mikko Hupa:** Conceptualization. **Zhongshan Li:** Supervision. **Peter Glarborg:** Methodology, Writing – review & editing. **Paul Marshall:** Methodology. **Marcus Aldén:** Project administration.

Declaration of Competing Interest

The authors declare that they have no known competing financial interests or personal relationships that could have appeared to influence the work reported in this paper.

Data availability

Data will be made available on request.

Acknowledgment

This study was financed by the Academy of Finland through the project Chemical challenges in gasification of biomass and waste (321598 and 353318) and Swedish Energy Agency through the KC-CECOST project (22538-4, biomass). PM acknowledges computational facilities provided by the National Science Foundation, Grant CHE-1531468.

Appendix A. Supplementary data

Supplementary data to this article can be found online at https://doi.org/10.1016/j.fuel.2022.126337.

References

[1] Hinidyarti L, Frandsen F, Livbjer H, Glarborg P, Marhsall P. An exploratory study of alkali sulfate aerosol formation during biomass combustion. Fuel 2008;87:1591–600.
[2] Christensen KA, Livbjerg H. A Plug Flow Model for Chemical Reactions and Aerosol Nucleation and Growth in an Alkali-Containing Flue Gas. Aerosol Sci Tech 2000;33(6):470–89.
[3] Jensen JR, Nielsen LB, Schultz-Møller C, Wedel S, Livbjerg H. The Nucleation of Aerosols in Flue Gases with a High Content of Alkali – A Laboratory Study. Aerosol Sci Technol 2000;33(6):490–509.
[4] Hupa M, Karlström O, Vainio E. Biomass combustion technology development – It is all about chemical details. Proceeding of the Combustion Institute 2017:113–34.
[5] Paulauskas R, Striūgas N, Sadeckas M, Sommersacher P, Retschitzegger S, Kienzl N. Online determination of potassium and sodium release behaviour during single particle biomass combustion by FES and ICP-MS. Sci Total Environ 2020;746:141162.
[6] Olsson JG, Jäglid U, Pettersson JBC. Alkali Metal Emission during Pyrolysis of Biomass. Energ Fuel 1997;11:779–84.
[7] Backman R, Frederick WJ, Hupa M. Basic Studies on Black-Liquor Pyrolysis and Char Gasification. Bioresource Technol 1993;46:153–8.
[8] Dayton DC, Frederick WJ. Direct Observation of Alkali Vapor Release during Biomass Vombustion and Gasification. 2. Black Liquor Combsution at 1100 °C. Energ Fuel 1996;10:284–92.
[9] Gilbe C, Öhman M, Lindström E, Boström D, Backman R, Samuelsson R, et al. Slagging Characteristics during Residential Combustion of Biomass Pellets. Energ Fuel 2008;22:3536–43.
[10] Lapuerta M, Acosta A, Pazo A. Fouling Deposits from Resiudal Biomass with High Sodium Content in Power Plants. Energ Fuel 2015;29:5007–17.
[11] Niu Y, Tan H, Hui S. Ash-related issues during biomass combustion: Alkali-induced slagging, silicate melt-induced slagging (ash fusion), agglomeration, corrosion, ash utilization, and related countermeasures. Prog Energ Combust 2016;52:1–61.
[12] Enestam S, Bankiewicz D, Tuiremo J, Mäkelä K, Hupa M. Are NaCl and KCl equally corrosive on superheater materials of steam boilers? Fuel 2013;104:294–306.
[13] Wu H, Yrjas P, Vainikka P, Lindberg D, Hupa M. Sulfation of alkali halides in a bench-scale bubbling fluidized bed reactor. Fuel 2016:173–9.

[14] Kassman H, Pettersson J, Steenari B-M, Åmand L-E. Two strategies to reduce gaseous KCl and chlorine in deposits during biomass combustion – injection of ammonium sulphate and co-combustion with peat. Fuel Process Technol 2013;105:170–80.
[15] Wu, H.; Wang, G.; Jensen, P. A.; Jappe Frandsen, F.; Glarborg, P. Reactive additives for alkali capture in biomass combustion. *Paper presented at 27th International Conference on the Impact of Fuel Quality on Power Production and the Environment, ,* **2018.**
[16] Aho M, Paakkinen K, Taipale R. Destruction of alkali chlorides using sulphur and ferric sulphate during grate combustion of corn stover and wood chip blends. Fuel 2013;103:562–9.
[17] Aho M, Vainikka P, Taipale R, Yrjas P. Effective new chemicals to prevent corrosion due to chlorine in power plant superheaters. Fuel 2008;87:647–54.
[18] Iisa K, Lu Y, Salmenoja K. Sulfation of Potassium Chloride at Combustion Conditions. Energ Fuel 1999;13:1184–90.
[19] Boonsongsup L, Iisa K, Frederick WJ. Kinetics of the Sulfation of NaCl at Combustion Conditions. Ind Eng Chem Res 1997;36:4212–6.
[20] Capablo J, Ballester J. Experimental study of the kinetics of sulfation of alkali chloride deposits. Fuel Process Technol 2015;140:215–21.
[21] Glarborg P, Marshall P. Mechanism and modeling of the formation of gaseous alkali sulfates. Combsut Flame 2005;141:22–39.
[22] Jiménez S, Ballester J. Influence of operating conditions and the role of sulfur in the formaiton of aerosols from biomass combustion. Combust Flame 2005;140:346–58.
[23] Ekvall T, Andersson K, Leffler T, Berg M. K-Cl-S chemistry in air and oxy-combustion atmospheres. Proceeding of the Combustion Institute 2017;36:4019–26.
[24] Ekvall T, Normann F, Andersson K, Johnsson F. Modeling the Alakli Sulfation Chemistry of Biomass and Coal Co-firing in Oxy-fuel Atmospheres. Energ Fuel 2014;28:3486–94.
[25] Li B, Sun Z, Li Z, Aldén M, Jakobsen FG, Hansen S, et al. Post-flame gas-phase sulfation of potassium chloride. Combust Flame 2013;160:959–69.
[26] Weng W, Chen S, Wu H, Glarborg P, Li Z. Optical Investigation of gas-phase KCl/KOH sulfation in post flame conditions. Fuel 2018;224:461–8.
[27] Weng W, Leffler T, Brackmann C, Aldén M, Li Z. Spectrally Resolved Ultraviolet (UV) Absorption Cross-Sections of Alkali Hydroxide and Chlorides Measured in Hot Flue Gases. Appl Spectrosc 2018;72(9):1388–95.
[28] Weng W, Li Z, Wu H, Aldén M, Glarborg P. Quantitative K-Cl-S chemistry in thermochemical conversion processes using in situ optical diagnostics. In: Proceeding of the Combustion institute 38th; 2021. p. 5219–27.
[29] Li, K.; Yan, W.; Yu, L.: Huangh, X.; Chen, Y.; Zhou, H.; Zheng, S.; Lou, C. Simultaneous Determination of Na Concentration and Temperature during Zhundong Coal Combustion using the Radiation Spectrum. *Energy Fuel.,* **2021**, 31, 3348-3359.
[30] Weng W. Optical Diagnostics for Quantitative Potassium Chemistry in Biomass Thermochemical Conversion Processes [Doctoral Thesis]. Department of Physics: Lund University, Lund; 2020.
[31] Weng W, Borggren J, Li B, Aldén M, Li Z. A novel multi-jet burner for hot flue gases of wide range of temperatures and compostions for optical diagnostics of solid fuels gasification/combustion. Rev Sci Instrum 2017;88:045104.
[32] Borggren J, Weng W, Hosseinnia A, Bengtsson P-E, Aldén M, Li Z. Diode laser-based thermometry using two-line atomic fluorsecnece of indium and gallium. Appl Phys B 2017;123:278.
[33] Weng W, Chang Y, Wu H, Glarborg P, Li Z. Optical measurements of KOH, KCl and K for quantitative K-Cl chemistry in thermochemical conversion processes. Fuel 2020;271:117643.
[34] Weng W, Brackmann C, Leffler T, Aldénr M, Li Z. Ultravioet Absorption Corss Sections of KOH and KCl from Nonintrusice Species-Specific Quantitative Detection in Hot Flue Gases. Anal Chem 2019;91(7):4719–26.
[35] Curtiss LA, Pedfern PC, Raghavachari K. Gausian-4 theory. J Chem Phys 2007;126:084108.
[36] Chase MW. NIST-JANAF Thermodynamic Tables. J Phys Chem Ref Data 1998;1–1951.
[37] Jiménez S, Ballester J. Formation and Emission of Submicron Particles in Pulverized Olive Residue (Orujillo) Combustion. Aerosol Sci Technol 2004;38:707–23.
[38] Christensen K, Livbjerg H. A Field Study of Submicron Particles from the Combustion of Straw. Aerosol Sci Technol 1996;25:185–99.
[39] Steinberg M, Schofield K. The chemistry of sodium with sufur in flames. Prog Energy Combust Sci 1990;16(4):311–7.